Journal of
Materials Chemistry A

Accepted Manuscript

This article can be cited before page numbers have been issued, to do this please use: X. Wang, X. Zhao, W. Dong, X. Zhang, Y. Xiang, Q. Huang and H. Chen, *J. Mater. Chem. A*, 2019, DOI: 10.1039/C9TA04018H.

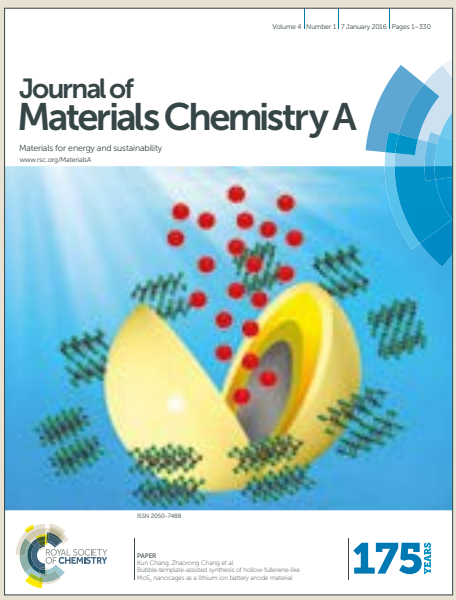

ROYAL SOCIETY OF CHEMISTRY

rsc.li/materials-a

View Article Online
DOI: 10.1039/C9TA04018H

ARTICLE

Integrating Amino Groups within Conjugated Microporous Polymers by Versatile Thiol-yne Coupling for Light-driven Hydrogen Evolution

Received 00th January 20xx,
Accepted 00th January 20xx

DOI: 10.1039/x0xx00000x

Xuepeng Wang,[a, b] Xiaodong Zhao,[a] Wenbo Dong,[a] Xiaohu Zhang,[a] Yonggang Xiang,*[a] Qiaoyun Huang,[b] Hao Chen *[a]

Conjugated microporous polymers (CMPs) are emerging as promising catalysts for photocatalytic hydrogen evolution, but hydrophobic surface and less active site exposure severely limit their efficiency. Herein, we contribute an effective and versatile strategy to function CMPs with abundant amino groups via radical thiol-yne reaction. As a result, the modified CMPs retain the light absorption ability and morphology, and better water compatibility along with more active sites exposure may accelerate subsequent proton reduction under visible light irradiation (λ > 420 nm). The hydrogen evolution rate (HER) and apparent quantum yields (AQYs) at 420 nm of modified CMPs were increased up to 27.2 times and 47.1 times in comparison to original CMPs. Photocatalytic H_2 evolution activity evaluation of BBT-SC2CH3, BBT-SC2N$(CH_3)_2$ and SC2NHAc in which amino groups were replaced with methyl, dimethyl amino or *N*-acetyl group revealed the crucial role of nitrogen, and aliphatic chain length between sulfur and nitrogen also proved important. Therefore, this protocol provides good opportunities for designing advanced CMPs and expands their application as photocatalyts for energy conversion.

Introduction

Rapid development of semiconductor-based photocatalysts makes direct solar-to-hydrogen conversion be a very promising approach to mitigate the energy crisis.[1-3] To increase utilization efficiency of solar energy, major efforts have been devoted to the exploration of inorganic semiconductor photocatalysts until photocatalytic water splitting ability of polymeric carbon nitride (C_3N_4) was discovered,[4] and then a variety of C_3N_4 and its derivatives have been fabricated in order to reach higher photocatalytic H_2 evolution rate (HER).[5-9] Very recently, it was also found that microporous and linear conjugated polymers synthesized *via* traditional organic polycondensation reactions could also act as photocatalysts for light driven H_2 evolution.[10-18] In contrast to structural stiffness of C_3N_4, controllable molecular engineering renders this kind of fully π conjugated polymers intrinsic advantages,[19] and microporous structures and high surface areas of conjugated microporous polymers (CMPs) also make them gain enormous attentions.[20-25]

Based on photocatalytic H_2 evolution process, better water compatibility and more exposed active sites of photocatalysts are favorable to HER increase.[26] In this regard, hydroxyl or amino grafted C_3N_4 exhibited superior photocatalytic H_2 evolution performance, meanwhile, aminated linkers (-NH_2) can act as hole stabilizer for metal-organic frameworks (MOF) based photocatalysts.[27-30] A recent work revealed that oxygen-containing and amino groups will increase hydrophilicity and prolong the excited electron lifetime of C_3N_4, [31] and the Lewis basicity of amino groups also benefits the photocatalytic reduction of H_2 and CO_2.[32, 33] Similarly, strategy of designing water dispersible conjugated polymer nanoparticles (PDots) has recently been utilized to significantly improve the photocatalytic HER of single-component polymers.[34-36] For most reported CMPs, the hydrophobic surface and less active sites exposure may hinder the proton to easily approach the active sites of the photocatalyst. In general, Sonogashira cross-coupling polycondensation was commonly employed to prepare CMPs, as a result, these CMPs contain abundant internal and terminal triple bonds.[37] By means of post-modification strategy, radical thiol-yne chemistry has been successfully applied to afford CMPs derivatives, in which C-S and C=C bonds forms,[38, 39] meanwhile, specific functional groups could also be integrated simultaneously for various applications.[40-42]

In this work, our previously reported conjugated microporous polymer BBT was first investigated. Thiol-yne reaction between BBT and cysteamine (SC2NH2) gave rise to BBT-SC2NH2, and aminated linkers were incorporated. Under visible light irradiation (λ > 420 nm), HER of BBT-SC2NH2 is 27.2 times higher than that of BBT, and apparent quantum yields (AQYs) of BBT-SC2NH2 at 420 nm reached 3.3% comparing to 0.07% of BBT. After the terminal NH_2 was protected by two methyl groups (BBT-SC2N$(CH_3)_2$) or acetyl group (BBT-SC2NHAc), no significant decrease of photocatalytic activities

[a] College of Science, Huazhong Agricultural University, Wuhan 430070, China. E-mail: hchenhao@mail.hzau.edu.cn; ygxiang@mail.hzau.edu.cn. Phone/Fax: +86-27-8728-8246
[b] Key Laboratory of Arable Land Conservation (Middle and Lower Reaches of Yangtze River), Ministry of Agriculture, College of Resources and Environment, Huazhong Agricultural University, Wuhan, 430070, China
Electronic Supplementary Information (ESI) available: [details of any supplementary information available should be included here]. See DOI: 10.1039/x0xx00000x

View Article Online
DOI: 10.1039/C9TA04018H

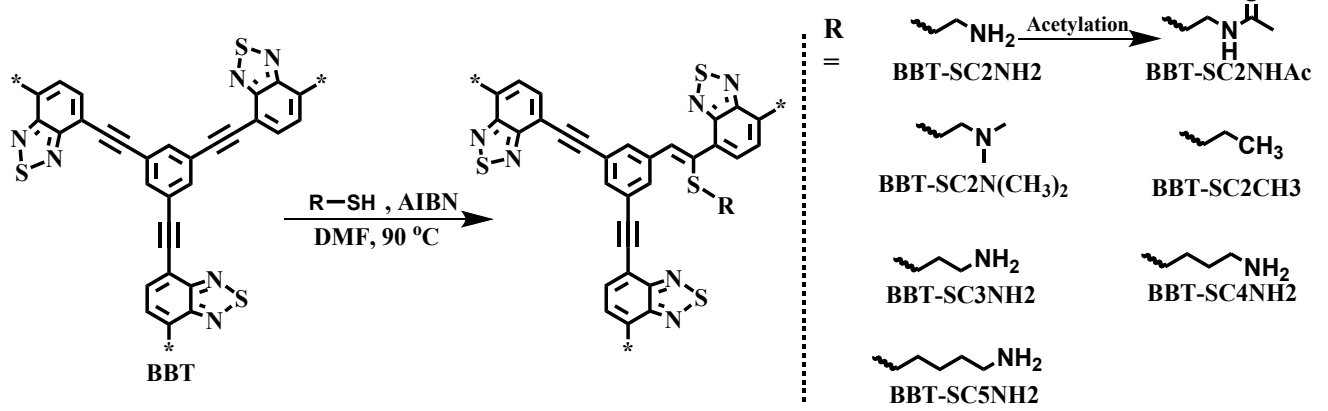

Scheme 1 The synthetic route of thiol-yne coupling functionalized BBT and their possible structures. Reaction conditions: 0.5 equiv. AIBN, 4 equiv. thiol per theoretical triple bonds, DMF, 90 °C, 24 h. AIBN = azodiisobutyronitrile.

was observed. Moreover, replacement of NH_2 by methyl group ($-CH_3$) resulted in low HER similar to BBT, suggesting the pivotal role of nitrogen. However, growth of chain length between sulfur and nitrogen severally damaged the activity. Inspired by above results, photocatalytic H_2 performance of two more amino functionalized PB-SC2NH2 and TB-SC2NH2 were also evaluated, and HER and AQY for both PB and TB have been increased significantly, revealing the versatility of thiol-yne post-modified strategy for the design of efficient CMP-based photocatalysts.

Experimental section

Materials

All comercially availale chemicals were received in analytic grade without further purification unless otherwise specified. 1,3,5-triethynylbenzene was synthesized via Sonogashira-Hagihara cross-coupling polycondensation and trimethylsilyl deprotection steps.

Post-modification of conjugated microporous polymers

BBT, PB and TB were synthesized according to Sonogashira-Hagihara cross-coupling polycondensation, and the details could be found in the Supporting Information.

CMPs-SC2NH2_4: CMP, cysteamine (4.0 equiv. per triple bond) and AIBN (0.5 equiv. per triple bond) were dissolved in certain volume of anhydrous DMF. After being degassed with Ar for 15 min, the resulting mixutres was stirred at 90 °C for 24 h. The solid was then collected by filtration and washing with hot methanol and acetone, and the final modified CMPs were afforded by drying in vacuum at 60 °C.

BBT-SC2NHAc: To the solution of BBT-SC2NH2 (100 mg) in CH_2Cl_2 was added excessive Ac_2O (1.02 g, 10 mmol) and triethylamine (2.02 g, 20 mmol), the resulting mixutre was stirred at room temperature under Ar for 24 h. The solid was collected by filtration and washing with CH_2Cl_2, and the acylation product was obtained by drying in vacuum at 60 °C.

Characterization

Fourier transform infrared (FT-IR) spectra were recorded on Nicolet FT-IR spectrometer, and pressed pellet was prepared by mixing KBr and the sample. Solid state ^{13}C cross-polarization magic angle spinning (CP/MAS) NMR spectra were measured on Bruker Avance spectrometer (400 MHz). Thermogravimetric analysis (TGA) was conducted on NETZSCH TG209 under air environment with a heating rate at 10 °C/min. Powder X-ray diffraction (PXRD) was taken on Bruker D8 advance using Cu K_α radiation. Scanning electron microscope (SEM) and transmission electron microscope (TEM) were measured on Hitachi SU8010 and Tecnai G2 F20 S-TWIN, respectively. UV-vis diffuse reflectance spectra (DRS) were taken on Shimadzu UV-3100. The steady-state photoluminescence (PL) measurements were carried out on Hitachi F-4600. Time resolved fluorescence spectra were achieved on Edinburgh Instruments F35 spectrofluorometer. The specific Brunauer-Emmett-Teller (BET) surface area and pore volumes were determined by N_2 sorption isotherms on Micrometrics ASAP 2040. Inductively coupled plasma-mass spectrometry (ICP-MS) measurement was carried out on Agilent 7900.

Electrochemical measurement

The electrochemical measurements were performed on the CHI660E workstation (Chenhua Instruments, China), and the standard three-electrode system includes platinum plate as the counter electrode, Ag/AgCl electrode as the reference electrode, and a working electrode. The working electrode was prepared as follows: 15 mg of each sample was thoroughly mixed with 200 μL isopropanol containing 5% Nafion, and the resulting suspension was carefully loaded on the ITO glass substrate (10 × 2.5 × 1.1 mm) and dried at 60 °C under vacuum for 1 h. 0.1 M Na_2SO_4 aqueous solution acted as the electrolyte for the photocurrent test while the aqueous solution of 0.1 M KCl and 0.005 M $K_3[Fe(CN)_6]$ was employed as the electrolyte for the electrochemical impedance spectroscopy (EIS) measurement. For cyclic voltammetry (CV) measurement, 0.1 M $TBAPF_6$ in CH_3CN solution was used as the electrolyte. The HOMO energy levels (E_{HOMO}) was calculated from onset oxidation potentials of CV curves according to the equation: $E_{HOMO} = -(E^{ox} + 4.8\ eV\ (v\ Ag/Ag^+) - E^{ox}_{Fc/Fc+})$, and $E^{ox}_{Fc/Fc+}$ is the oxidation potential of ferrocene/ferrocenium (Fc/Fc^+) couple for the calibration. The Standard Hydrogen Electrode (SHE) could be derived from: E_{HOMO} (SHE) = – 4.5 eV - E_{HOMO}, E_{LUMO} (SHE) = E_{HOMO} (SHE) – E_g.

Photocatalytic H_2 production procedure

The photocatalytic reaction was carried out in a Pyrex top-irradiation vessel with a closed gas circulation system, and 300 W Xe-lamp (PLS

SXE300/300UV, Beijing Perfectlight Technology Inc. Ltd, China) equipped with a UV cut-off (λ > 420 nm) filter was used as the light source. In a typical procedure: 30 mg catalyst was dispersed in a fresh aqueous solution (30 mL) containing 10 vol% triethanolamine (TEOA). After being sonicated for 10 min, the solution was then transferred in the reaction vessel and vacuumed for 10 min before photocatalytic reaction. After irradiation for 1 h, the efficiency of released H_2 was calculated by gas chromatography (SP7820, 5 Å molecular sieve columns, Ar carrier, and TCD detector)

The apparent quantum yield (AQY) experiments were performed according to the photocatalytic reaction, in which UV cut-off (λ > 420 nm) filter was replaced by band-pass filter (λ = 420, 450 nm, etc.) in order to achieve monochromatic light. The AQY was calculated by the following formula: AQY % = (2 * number of evolved H2 molecules) % / (number of incident photons).

Results and discussion

BBT was synthesized via Sonogashira-Hagihara coupling reaction between 4,7-dibromobenzo[*c*][1,2,5]thiadiazole and 1,3,5-triethynylbenzene according to the reported procedure.[43] As shown in scheme 1, the thiol-yne modification of BBT was carried out with varying amount of cysteamine using azoisobutyronitrile (AIBN, 0.5 equiv. per thiol) as a radical initiator, and the sulfur functionalized BBT-SC2NH2_X was afforded, where X represents the molar ratio of cysteamine to theoretical amount of alkyne in BBT. It should be noted that not all of the -C≡C- bonds involves the thiol-yne reaction, and only one possible structure of modified-BBT is shown in scheme 1.

The successful synthesis of functionalized BBT-SC2NH2_4 was first estimated by solid state ^{13}C cross-polarization magic angle spinning (CP/MAS) NMR. As shown in Fig. 1a, there emerged new characteristic aliphatic carbon signals of cysteamine moieties at around 30.8 ppm and 38.8 ppm in comparison to that of unmodified BBT. Meanwhile, the FT-IR spectra of BBT before and after cysteamine functionalization were further compared (Fig. 1b), a strong and broad band arises at ~1660 cm^{-1}, which was attributed to the generation of C=C bonds after thiol-yne reaction. There also newly appeared peaks at ~3400 cm^{-1} which corresponded to N-H stretching vibration of the amino groups ($-NH_2$), and the strong signals of -C≡C- at 2200 cm^{-1} still existed, indicating that cysteamine moieties could only be grafted to part of triple bonds despite excessive addition of thiol reactants. Both the samples before and after modification displayed very close decomposition temperature at *ca.* 343 °C under air atmosphere (Fig. S1), revealing that thiol-yne reaction doesn't impair the thermal stability despite the existence of aliphatic and amine groups.

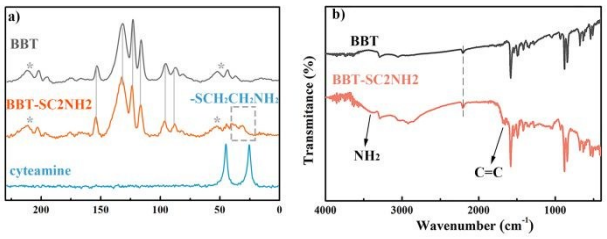

Fig. 1. (a) Solid state ^{13}C CP/MAS NMR spectra, * indicates the spinning side bands; (b) FTIR spectra of BBT and BBT-SC2NH2.

The surface compositions of as-prepared photocatalysts were further compared by X-ray photoelectron spectroscopy. For unmodified BBT, there was one main N1s peak with binding energy of 399.7 eV, which represented the nitrogen in the benzothiadiazole units (N-S-N), after thiol-yne reaction, an additional N1s peak at 400.4 eV was generated, which can be identified as the C-NH_2 (Fig. 2a) [44]. In the case of S2p, the binding energies of 166.9 eV and 165.7 eV for BBT were assigned to sulfur in the benzothiadiazole ring (N-S-N), and the new peak at 163.8 eV arose from new generated sulfur groups (C-S-C) for BBT-SC2NH2 (Fig. 2b). In the survey spectra, it can be seen that a decreasing carbon to sulfur ratio (C/S) was afforded for BBT-SC2NH2_4 in contrast to the original BBT (Fig. S2), which was in agreement with elemental analysis in which a slight increase of sulfur and nitrogen contents was observed (Table S1). Meanwhile, both BBT and BBT-SC2NH2_4 displayed similar amorphous structures without discernible crystalline peaks by powder X-ray diffraction (PXRD) measurements (Fig. S3). The Brunauer–Emmett–Teller (BET) surface area and pore sized distribution of BBT and sulfur functionalized BBT-SC2NH2 were compared by N_2 adsorption-desorption analysis (Fig. 2c, Table 1). Upon modification, the surface area increased from 110 $m^2\ g^{-1}$ to 148 $m^2\ g^{-1}$ without affecting the pore size diameter significantly (Fig. S4). As depicted in Fig. 2d, there was no observable change on the morphologies before and after thiol-yne reaction by scanning electron microscopy (SEM) and transmission electron microscopy (TEM) images, indicating that polymer framework kept intact.

No obvious colour change of BBT before and after thiol-yne reaction was detected, and it revealed that BBT and BBT-SC2NH2 may had very similar light absorption ability, which was further investigated by UV–vis diffuse reflectance spectra (DRS). As shown in Fig. 3a, original BBT exhibited visible light absorption ability. For BBT-SC2NH2, there appeared slight red-shift ranging from 460 nm to 520 nm while the absorption curve below 460 nm was not affected. BBT seemed to show stronger light absorption ability in the range from

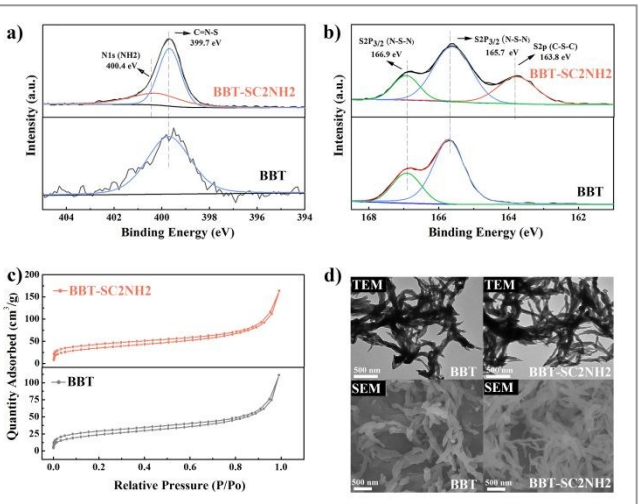

Fig. 2. High-resolution XPS spectra of N1s (a) and S2p (b); (c) Nitrogen adsorption and desorption isotherm curves; (d) TEM and SEM images comparison of BBT and BBT-SC2NH2.

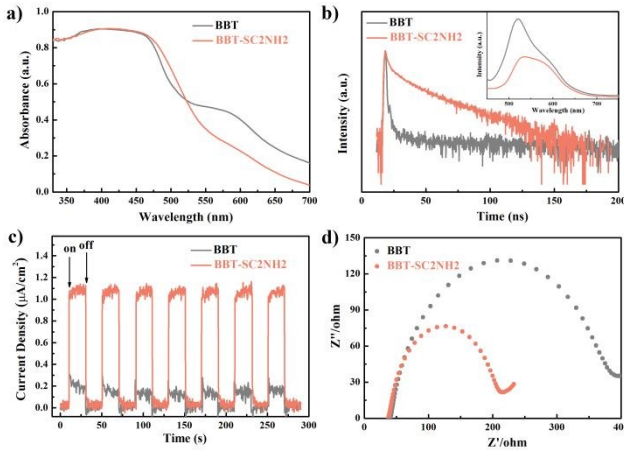

Fig. 3. (a) UV–vis diffuse reflectance spectra; (b) time-resolved photoluminescence decay spectra (the inset shows the photoluminescence spectra with the excitation wavelength at 415 nm); (c) photocurrent curves versus time; (d) electrochemical impedance spectroscopy plots of BBT and BBT-SC2NH2.

520 nm to 700 nm, but the absorption tail of BBT in the longer wavelength might be caused by light scattering due to intrinsic amorphous properties of the conjugated polymers. The optical bandgaps (E_g) of BBT and BBT-SC2NH2 were determined to be 2.71 eV and 2.61 eV according to Kubelka-Munk function, respectively (Table 1 and Fig. S6a). The highest occupied molecular orbital (HOMO) levels are calculated by cyclic voltammetry (CV) curves (Fig. S6b), and then lowest unoccupied molecular orbital (LUMO) levels could be achieved by E_g and HOMO levels. It turns out that thiol-yne functionalization has no significant impact on the absorption ability and redox potential of BBT.

It is well accepted that the charge transfer properties are crucial factors determining the photocatalytic performance,[45] and the transfer efficiency of photogenerated carries before and after thiol-yne reaction was first examined by photoluminescence (PL) spectra under the excitation wavelength of 415 nm. As shown in Fig. 3b, PL intensity of modified BBT-SC2NH2 was dramatically quenched in comparison to BBT, indicating lower recombination possibility of photo-generated electron–hole pairs. Next, time-resolved transient

Table 1 Porosity parameters and electrochemical properties of CMPs and CMP-SC2NH2

Polymers	S_{BET} [a] ($m^2 g^{-1}$)	LUMO [b]/HOMO [c] (V vs NHE)	E_g [d] (eV)	HER [e] (μmol/h)	AQY [f] (420nm)
BBT	110	-1.00/1.71	2.71	10	0.07
BBT-SC2NH2	148	-0.91/1.70	2.61	272	3.3
PB	144	-0.51/1.50	2.01	42	0.29
PB-SC2NH2	121	-0.65/1.38	2.03	335	1.87
TB	529	-1.09/1.46	2.55	21	0.05
TB-SC2NH2	436	-1.12/1.45	2.57	86	0.5

[a] Surface area was calculated from the N_2 adsorption isotherms via BET method. [b] $E_{LUMO} = E_{HOMO} - E_g$. [c] Determined using cyclic voltammetry. [d] Optical gap was determined from the onset of absorption spectrum. [e] Reaction conditions: 30 mg of polymer suspended in 30 mL 10 vol% TEOA/H_2O, irradiated using 300-W Xe lamp with bandpass filter λ > 420 nm. [f] AQY was measured with bandpass filter at 420 nm.

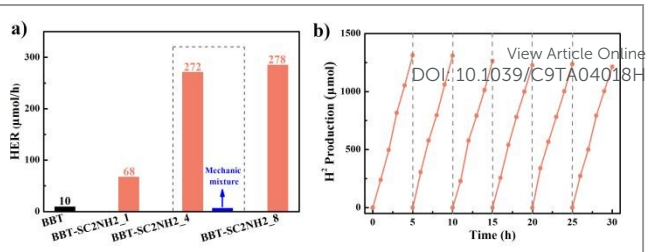

Fig. 4. (a) Photocatalytic H_2-production activities of BBT, BBT-SC2NH2_1, BBT-SC2NH2_4, BBT-SC2NH2_8, and the mechanic mixture of BBT, 0.5 equiv. AIBN and 4 equiv. cysteamine; (b) Long-term stability test of H_2 production for BBT-SC2NH2_4 in six successive runs over total 30 h under visible light irradiation (λ > 420 nm).

PL decay was further utilized to confirm the better transfer efficiency of charge carriers. By the multi-exponential fitting, it was found that the average lifetime increases from 0.75 ns of BBT to 2.12 ns of BBT-SC2NH2, and the longer lifetime would be beneficial to photocarriers transfer. Meanwhile, transient generation of photocurrent and electrochemical impedance spectroscopy (EIS) measurements were conducted to evaluate the photogenerated carriers' migration across the interfaces of the samples. As shown in Fig. 3c and Fig. 3d, BBT-SC2NH2 showed a comparatively enhanced photocurrent intensity than unmodified counterparts, and it indicated that sulfur functionalization will contribute to promoted mobility of photo-generated charge carriers. In the EIS Nyquist plots, a remarkable decrease in the arc radius for BBT-SC2NH2 was observed, further confirming that charge transfer resistance of BBT-SC2NH2 was weaker than BBT, and thus superior photocatalytic performance may be expected after thiol-yne reaction.

Following the successful synthesis of the sulfur functionalized BBT-SC2NH2 and initial acquirement of electron transfer results, we moved to measure photocatalytic water splitting efficiency of unmodified BBT and modified BBT-SC2NH2. The evaluation was performed for our catalysts under visible light irradiation (λ > 420 nm), and triethanolamine (TEOA) acted as a sacrificial electron donor. As shown in Fig. 4a, BBT had very low H_2 evolution rate (HER) of ~10 umol h^{-1}. To our delight, photocatalytic H_2 evolution activity of BBT-SC2NH2_1 was enhanced significantly by 6.8 times with HER at ~68 umol h^{-1}. As the molar ratio of cysteamine to theoretical alkyne content in BBT continued to increase, HER of BBT-SC2NH2_4 reached up to ~272 umol h^{-1} (9.06 mmol g^{-1}). In contrast, performance of BBT-SC2NH2_8 was comparable to BBT-SC2NH2_4, indicating that 4 equivalence of cysteamine in the thiol-yne reaction was enough to afford the best functionalized BBT-SC2NH2 in this designed system. Furthermore, the photocatalytic activity of the mechanical mixture BBT/cysteamine/AIBN was also evaluated, and it turned out that direct addition of the reactants and catalysts will not improve the performance of original BBT, indicating crucial modification strategy by thiol-yne coupling. Meanwhile, the apparent quantum yields (AQYs) of BBT and BBT-SC2NH2_4 were compared under same monochromatic incident light, and an AQY of 3.3% at 420 nm was achieved for BBT-SC2NH2_4, increased by marvellous 47.1 times in contrast to BBT with AQY of 0.07%. Moreover, AQY measurement in all the wavelength region was compared, the higher AQY values BBT-SC2NH2_4 under various

View Article Online
DOI: 10.1039/C9TA04018H

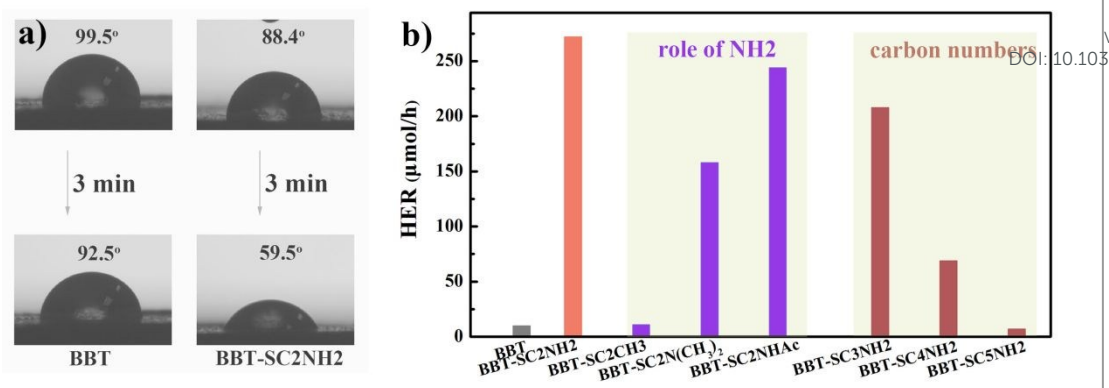

Fig. 5. (a) Water contact angle measurements of BBT and BBT-SC2NH2 over 3 min; (b) comparison of photocatalytic H_2-production activities.

monochromatic incident light was consistent with its superior photocatalytic H_2 production activities (Fig. S7).

Next, long-term photocatalytic activity of BBT-SC2NH2_4 was evaluated in the same condition. As can be seen in Fig. 4b, steady hydrogen evolution is observed in six consecutive runs over total 30 hours. The chemical structure of BBT-SC2NH2_4 before and after irradiation was characterized by FT-IR (Fig. S8), and it indicated that both the functional groups and intrinsic conjugated skeletons were kept in the same state, verifying excellent recyclability and photocorrosion-resistance of BBT-SC2NH2. It was noted that the as-prepared CMPs exhibited photocatalytic H_2 production activity without additional Pt cocatalyst, very recently, and it has been proved that less than 40 ppm of residual Pd in the conjugated polymers was sufficient to play the role of co-catalyst in the photocatalytic process.[46] In our experiments, residual Pd content of BBT was determined to be *ca.* 0.5% by inductively coupled plasma mass spectrometry (ICP-MS), but the Pd concentration between BBT and BBT-SC2NH2 was almost same, suggesting that enhanced photocatalytic activity after thiol-yne modification was caused by intrinsic merits of its chemical composition.

As being discussed previously, there only appeared subtle change of light absorption ability and BET surface area before and after sulfur functionalization, thus dramatic enhancement in photocatalytic H_2 evolution ability of functionalized BBT-SC2NH2 should arise from some other reasons. Due to the potential hydrogen bond formation between amine group and water, the surface hydrophilicity was first evaluated by water contact angle measurement. As shown in Fig. 5a, unmodified BBT showed initial contact angle of 99.5°, which decreased slightly to 92.5° over the next 3 min. In contrast, BBT-SC2NH2_4 displayed an obvious lower contact angle of 88.4° with a much faster decrease rate, and the angle finally reached 59.5° after 3 min. it was definitely expected that introduction of SC2NH2 with amino groups resulted in more hydrophilic surface of BBT-SC2NH2 *via* thiol-yne reaction, which should be beneficial to water adsorption. Subsequently, we also compared the water compatibility of polymers in TEOA/H_2O, and it turned out that CMP-SC2NH2 can kept good dispersion state without apparent self-aggregation after long-time irradiation, which was also the prerequisite of steady hydrogen evolution in long term.

To further figure out the role of NH_2 group, BBT-SC2CH3 was then designed by thiol-yne reaction between BBT and 3-propanethiol, and BBT-SC2CH3 showed a comparable HER to BBT. In comparison to BBT-SC2NH2, it was inferred that only existence of sulfur would not affect the photocatalytic activity, and NH2 from cysteamine moieties should contributed mainly to the superior performance of BBT-SC2NH2. To exclude the possibility that H atom of generated H_2 molecule came from NH_2 group, BBT-SC2N$(CH_3)_2$ in which two H of NH_2 were replaced by two CH_3 groups was also prepared, and it revealed that HER decreased from 272 μmol h^{-1} to 158 μmol h^{-1}, which may be caused by incorporation of additional methyl group that hindered the interaction between nitrogen and water. On the other hand, BBT-SC2NH2 further reacted with acetic anhydride (Ac_2O) to afford BBT-SC2NHAc. The structure of BBT-SC2NHAC has been identified by solid ^{13}C NMR (Fig. S10), and there

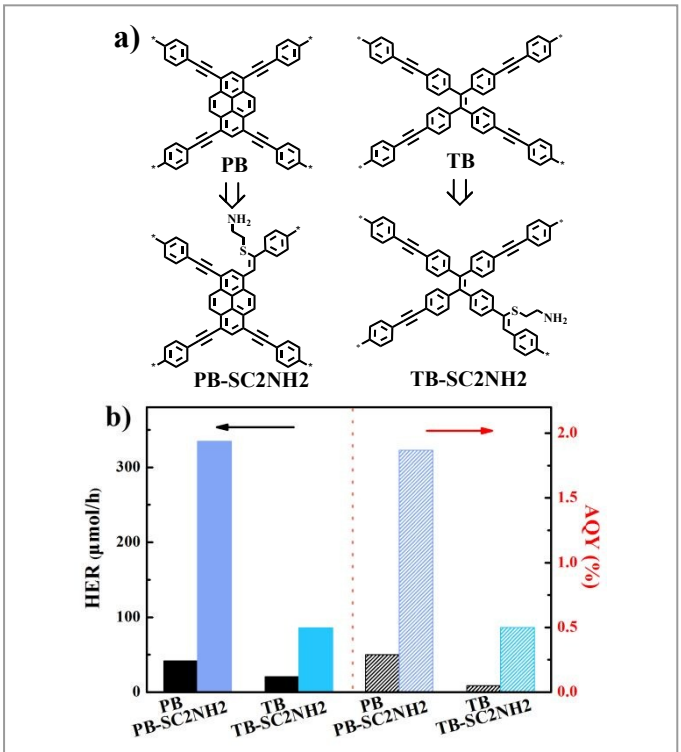

Fig. 6. (a) Synthesis of PB-SC2NH2 and TB-SC2NH2 by thiol-yne reaction; (b) photocatalytic H_2-production activities of PB and TB before and after thiol-yne reaction.

appeared two new peak at 170.1 ppm and 22.3 ppm which were assigned to carbonyl and methyl of acetyl group, respectively. As expected, BBT-SC2NHAc exhibited a comparable HER (244 μmol h^{-1}) to BBT-SC2NH2 as there still existed strong intermolecular H bond formation between amide group and H_2O. Accordingly, it was inferred that NH_2 was not the source of H in the generated H_2 molecule, but the hydrogen bonding played a critical role in improving photocatalytic hydrogen production. [47]

Next, we wonder if the chain length between sulfur and nitrogen would impact the photocatalytic activity, and then BBT-SC3NH2, BBT-SC4NH2, BBT-SC5NH2 were further designed in which 3-aminopropane-1-thiol, 4-aminobutane-1-thiol, 5-aminopentane-1-thiol were thiol reactants. As shown in Fig. 5b, while the aliphatic chain length was extended from 2 to 3, BBT-SC3NH2 had a decreased HER of 208 μmol h^{-1}. As the chain length continued to grow, photocatalytic activity was rapidly decreased. HER of BBT-SC4NH2 was reduced to 69 μmol h^{-1}, and BBT-SC5NH2 even had lower HER than non-functionalized BBT. It was assumed that sequential addition of carbon atoms between sulfur and NH_2 led to decreased interaction between the polymer skeleton and amino groups, and then the role of NH_2 as the active site for further proton reduction in the process of photocatalytic H_2 evolution was weakened. Moreover, the impact of chain length between S and N on the photocurrent is also evaluated, and the intensity change was in good agreement with the HER activity (Fig. S12).

To verify the versatility of thiol-yne functionalization, two other porous conjugated polymers PB and TB were further designed, similarly, both of them were modified with cysteamine by thiol-yne reaction in which 4 molar equivalence of cysteamine per theoretical alkyne was used. After structures and optical properties of the as-prepared PB-SC2NH2 and TB-SC2NH2 were investigated by extensive characterizations (Fig. S13-Fig. S21), the photocatalytic activity was then evaluated. It turned out that PB-SC2NH2 also afforded a nearly 8.0 times higher HER than unmodified PB, reaching 335 μmol h^{-1}, and HER of TB-SC2NH2 was increased to 86 μmol h^{-1} in comparison to HER of 21 μmol h^{-1} for TB (Fig. 6b). Moreover, the AQY of these four conjugated polymers along with absorption wavelengths changes were measured, and it indicated that photocatalytic HER results were consistent with absorption ability in the visible light region. The maximal AQY value of PB and TB obtained at 420 nm was determined to be 0.27% and 0.05%, respectively, in contrast, maximal AQY of PB-SC2NH2 and TB-SC2NH2 were calculated to be 1.87%, 0.5% at 420 nm, improved by 6.4 and 10 times higher, respectively (Fig. 6b and Fig. S22).

Similarly, water contact angle measurements indicated that post-modification of PB and TB by cysteamine contributed to better surface wettability (Fig. S23 and Fig. S24), and a rapid decrease of contact angle for PB-SC2NH2 and TB-SC2NH2 was observed over 3 min, decreasing from 104.9° and 103.2° to 65.0° and 64.0°, respectively, which was much smaller than their original counterparts. Meanwhile, PB-SC2NH2 and TB-SC2NH2 had a lower recombination possibility of photogenerated electron–hole pairs by PL test (Fig. S25-Fig. S27), and photocurrent density and EIS measurement further confirmed that cysteamine modification of PB and TB by thiol-yne reaction led to more efficient charge carriers transfer. Accordingly, it can be seen that introduction of cysteamine into CMPs via thiol-yne reaction may provide a facile and efficient strategy for significant enhancement of their photocatalytic H_2 evolution performance (Table S2).

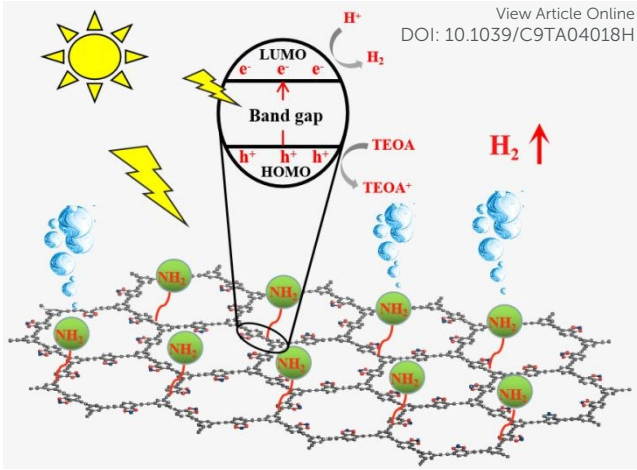

Fig. 7. Proposed photocatalytic H_2 evolution mechanism of the amino functionalized conjugated polymers.

Based on above discussion, the mechanism of photocatalytic hydrogen evolution for the amino functionalized conjugated polymers (CMPs-SC2NH2) is proposed (Fig. 7). Photogenerated electrons (e^-) jump to the LUMO level, and holes (h^+) form at the HOMO level. The electrons are further transferred to the surface of catalyst for H_2 evolution, and the holes are consumed by triethanolamine (TEOA). A significant increase of HER for the amino functionalized conjugated polymers can be explained as follows: (1) the introduced amino groups effectively promote the separation and transfer efficiency of photo-generated carriers, (2) More hydrophilic properties of incorporated amino groups are beneficial to interfacial reactions between polymers and water.

Conclusions

In summary, a radical thiol-yne coupling strategy has been successfully applied for post-modification of conjugated microporous polymers bearing triple bonds, without compromising optical bandgap and morphology, abundant amino groups were incorporated into the skeleton of the polymer. Under visible irradiation, all as-prepared CMPs-SC2NH2 exhibited superior photocatalytic H_2 evolution activity than their original CMPs, and steady HER and AQY at 420 nm of BBT-SC2NH2 reached up to 272 μmol/h and 3.3%, which were 27.2 times and 47.1 times higher than BBT, respectively. It was inferred that better water compatibility of CMPs-SC2NH2 benefited water compatibility and photogenerated charge separation, and the introduced amino groups prolonged electron lifetime, which eventually accelerated subsequent proton reduction. Moreover, the nitrogen, not the hydrogen in the introduced NH_2 groups proved to be pivotal for the enhanced photocatalytic activity, and aliphatic chain length between sulfur and nitrogen was also crucial to the performance. Accordingly, this works provides a versatile and facile post-modification method for designing highly efficient CMPs based photocatalysts.

Conflicts of interest

There are no conflicts to declare.

Acknowledgements

The research was financially supported by the National Natural Science Foundation of China (51572101, 51872107 and 51802107), and the Fundamental Research Funds for the Central Universities (2662017JC021, 2662015PY047 and 2662016PY088).

Notes and references

1. M. Q. Yang, M. Gao, M. Hong and G. W. Ho, *Adv. Mater.*, 2018, DOI: 10.1002/adma.201802894, e1802894.
2. F. Wang, Q. Li and D. Xu, *Adv. Energy Mater.*, 2017, **7**, 100529.
3. H. Park, H. I. Kim, G. H. Moon and W. Choi, *Energy Environ. Sci.*, 2016, **9**, 411-433.
4. X. C. Wang, K. Maeda, A. Thomas, K. Takanabe, G. Xin, J. M. Carlsson, K. Domen and M. Antonietti, *Nat. Mater.*, 2009, **8**, 76-80.
5. H. Ou, X. Chen, L. Lin, Y. Fang and X. Wang, *Angew. Chem. Int. Ed.*, 2018, **57**, 8729-8733.
6. Z. Guigang, L. Lihua, L. Guosheng, Z. Yongfan, S. Aleksandr, Z. Spiros, W. Xinchen and A. Markus, *Angew. Chem. Int. Ed.*, 2018, **57**, 9372-9376.
7. M. Zhu, S. Kim, L. Mao, M. Fujitsuka, J. Zhang, X. Wang and T. Majima, *J. Am. Chem. Soc.*, 2017, **139**, 13234-13242.
8. J. Fu, J. Yu, C. Jiang and B. Cheng, *Adv. Energy Mater.*, 2017, **7**, 1701503.
9. S. W. Cao, J. X. Low, J. G. Yu and M. Jaroniec, *Adv. Mater.*, 2015, **27**, 2150-2176.
10. J. Kosco and I. McCulloch, *ACS Energy Letters*, 2018, **3**, 2846-2850.
11. D. J. Woods, R. S. Sprick, C. L. Smith, A. J. Cowan and A. I. Cooper, *Adv. Energy Mater.*, 2017, **7**, 1700479.
12. S. Bi, Z.-A. Lan, S. Paasch, W. Zhang, Y. He, C. Zhang, F. Liu, D. Wu, X. Zhuang, E. Brunner, X. Wang and F. Zhang, *Adv. Funct. Mater.*, 2017, **27**, 1703146.
13. R. S. Sprick, B. Bonillo, R. Clowes, P. Guiglion, N. J. Brownbill, B. J. Slater, F. Blanc, M. A. Zwijnenburg, D. J. Adams and A. I. Cooper, *Angew. Chem. Int. Ed.*, 2016, **55**, 1824-1828.
14. C. Yang, B. C. Ma, L. Z. Zhang, S. Lin, S. Ghasimi, K. Landfester, K. A. I. Zhang and X. C. Wang, *Angew. Chem. Int. Ed.*, 2016, **55**, 9202-9206.
15. L. W. Li, Z. X. Cai, Q. H. Wu, W. Y. Lo, N. Zhang, L. X. Chen and L. P. Yu, *J. Am. Chem. Soc.*, 2016, **138**, 7681-7686.
16. R. S. Sprick, J. X. Jiang, B. Bonillo, S. J. Ren, T. Ratvijitvech, P. Guiglion, M. A. Zwijnenburg, D. J. Adams and A. I. Cooper, *J. Am. Chem. Soc.*, 2015, **137**, 3265-3270.
17. Y. G. Xiang, X. P. Wang, X. H. Zhang, H. J. Hou, K. Dai, Q. Y. Huang and H. Chen, *J. Mater. Chem. A*, 2018, **6**, 153-159.
18. X. H. Zhang, X. P. Wang, J. Xiao, S. Y. Wang, D. K. Huang, X. Ding, Y. G. Xiang and H. Chen, *J. Catal.*, 2017, **350**, 64-71.
19. Y. H. Xu, S. B. Jin, H. Xu, A. Nagai and D. L. Jiang, *Chem. Soc. Rev.*, 2013, **42**, 8012-8031.
20. Y. B. Zhou and Z. P. Zhan, *Chem. Asian J.*, 2018, **13**, 9-19.
21. N. Chaoui, M. Trunk, R. Dawson, J. Schmidt and A. Thomas, *Chem. Soc. Rev.*, 2017, **46**, 3302-3321.
22. Y. Xu, S. Jin, H. Xu, A. Nagai and D. Jiang, *Chem. Soc. Rev.*, 2013, **42**, 8012-8031.
23. G. G. Zhang, Z. A. Lan and X. C. Wang, *Angew. Chem. Int. Ed.*, 2016, **55**, 15712-15727.
24. W. Zhang, J. Tang, W. Yu, Q. Huang, Y. Fu, G. Kuang, C. Pan and G. Yu, *ACS Catal.*, 2018, DOI: 10.1021/acscatal.8b01478, 8084-8091.
25. J. Byun, W. Huang, D. Wang, R. Li and K. A. I. Zhang, *Angew. Chem. Int. Ed.*, 2018, **27**, 2967-2971.
26. X. B. Chen, S. H. Shen, L. J. Guo and S. S. Mao, *Chem. Rev.*, 2010, **110**, 6503-6570.
27. M. B. Chambers, X. Wang, L. Ellezam, O. Ersen, M. Fontecave, C. Sanchez, L. Rozes and C. Mellot-Draznieks, *J. Am. Chem. Soc.*, 2017, **139**, 8222-8228.
28. M. W. Logan, S. Ayad, J. D. Adamson, T. Dilbeck, H. B. Kenneth and F. J. Uribe-Romo, *J. Mater. Chem. A*, 2017, **5**, 11854-11863.
29. J. G. Santaclara, M. A. Nasalevich, S. Castellanos, W. H. Evers, F. C. M. Spoor, K. Rock, L. D. A. Siebbeles, F. Kapteijn, F. Grozema, A. Houtepen, J. Gascon, J. Hunger and M. A. van der Veen, *ChemSusChem*, 2016, **9**, 388-395.
30. J. Xu, J. Gao, C. Wang, Y. Yang and L. Wang, *Appl. Catal. B: Environ.*, 2017, **219**, 101-108.
31. N. N. Meng, J. Ren, Y. Liu, Y. Huang, T. Petit and B. Zhang, *Energy Environ. Sci.*, 2018, **11**, 566-571.
32. K. M. Cho, K. H. Kim, K. Park, C. Kim, S. Kim, A. Al-Saggaf, I. Gereige and H. T. Jung, *ACS Catal.*, 2017, **7**, 7064-7069.
33. Y. X. Li, H. Xu, S. X. Ouyang, D. Lu, X. Wang, D. F. Wang and J. H. Ye, *J. Mater. Chem. A*, 2016, **4**, 2943-2950.
34. P.-J. Tseng, C.-L. Chang, Y.-H. Chan, L.-Y. Ting, P.-Y. Chen, C.-H. Liao, M.-L. Tsai and H.-H. Chou, *ACS Catal.*, 2018, DOI: 10.1021/acscatal.8b01678, 7766-7772.
35. L. Wang, R. Fernández-Terán, L. Zhang, D. L. A. Fernandes, L. Tian, H. Chen and H. Tian, *Angew. Chem. Int. Ed.*, 2016, **128**, 12494-12498.
36. P. B. Pati, G. Damas, L. Tian, D. L. A. Fernandes, L. Zhang, I. B. Pehlivan, T. Edvinsson, C. M. Araujo and H. Tian, *Energy Environ. Sci.*, 2017, **10**, 1372-1376.
37. A. G. Slater and A. I. Cooper, *Science*, 2015, **348**, aaa8075.
38. H. Urakami, K. Zhang and F. Vilela, *Chem. Commun.*, 2013, **49**, 2353-2355.
39. B. Kiskan and J. Weber, *ACS Macro Lett.*, 2012, **1**, 37-40.
40. X. Han, M. Xu, S. Yang, J. Qian and D. Hua, *J. Mater. Chem. A*, 2017, **5**, 5123-5128.
41. J. G. Kim, M. C. Cha, J. Lee, T. Choi and J. Y. Chang, *ACS Appl. Mater. Interfaces*, 2017, **9**, 38081-38088.
42. K. Cho, S. M. Lee, H. J. Kim, Y.-J. Ko and S. U. Son, *J. Mater. Chem. A*, 2018, **6**, 15553-15557.
43. H. J. Hou, X. H. Zhang, D. K. Huang, X. Ding, S. Y. Wang, X. L. Yang, S. Q. Li, Y. G. Xiang and H. Chen, *Appl. Catal. B: Environ.*, 2017, **203**, 563-571.
44. L. N. Li, D. Cruz, A. Savateev, G. G. Zhang, M. Antonietti and Y. B. Zhao, *Appl. Catal. B: Environ.*, 2018, **229**, 249-253.
45. Y. Yu, W. Yan, X. F. Wang, P. Li, W. Y. Gao, H. H. Zou, S. M. Wu and K. J. Ding, *Adv. Mater.*, 2018, **30**, 1705060.
46. J. Kosco, M. Sachs, R. Godin, M. Kirkus, L. Francas, M. Bidwell, M. Qureshi, D. Anjum, J. R. Durrant and I. McCulloch, Adv. Energy Mater., 2018, 8, 1802181.
47. C. Q. Xu, Y. H. Xiao, Y. X. Yu and W. D. Zhang, *J. Mater. Sci.*, 2018, **53**, 409-422.

View Article Online
DOI: 10.1039/C9TA04018H

View Article Online
DOI: 10.1039/C9TA04018H

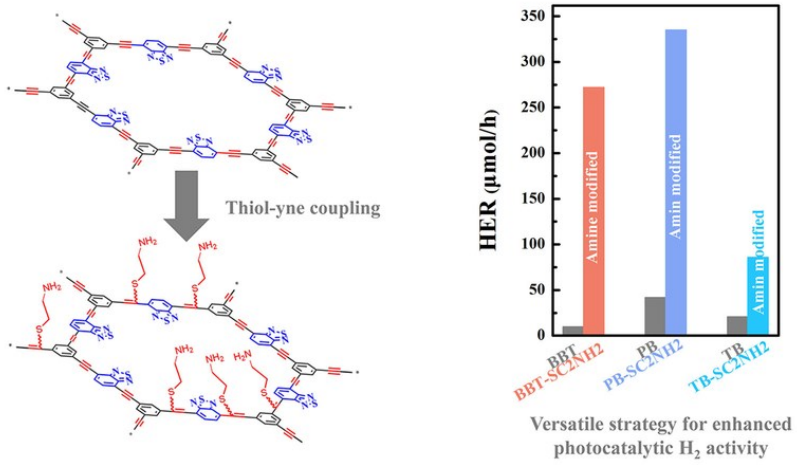

79x39mm (300 x 300 DPI)